# SEISMIC FRAGILITY ANALYSIS OF CONCRETE GRAVITY DAMS


**Yusof Ghanaat**
*Quest Structure, Inc. USA*

**Robert C. Patev**
*US Army Corps of Engineers, Risk Management Center, Institute for Water Resources, USA*

**Anjana K. Chudgar**
*US Army Corps of Engineers, Headquarters, Washington D.C., USA*

**ABSTRACT**
This paper introduces a practical methodology with example for development of seismic fragilities for concrete gravity dams using nonlinear time-history seismic analyses with Latin Hypercube Simulation (LHS). Sliding at the dam base and lift joints are identified as two prominent failure modes of the dam. Random and uncertainty input variables influencing the seismic fragility are generated using LHS and randomly selected to develop seismic fragilities for both failure modes. Nonlinear seismic analyses are performed for ten trials at several ground motion levels until each trial indicates failure. The ground motion variable includes ten sets of acceleration time histories obtained from the actual earthquake recordings and matched to a target response spectrum. The probability of failure for each random nonlinear trial is calculated as a function of the peak failure acceleration associated with the incipient sliding. The calculated results are used to obtain the best-fit distribution to the data.

*Keywords: Seismic fragility; Dam; Failure; Sliding; Lift joint*

## 1. INTRODUCTION

Seismic risk assessment of dams is a critical component of estimating social and economic loss from earthquakes and to mitigate losses when earthquakes occur. Risk and uncertainty are intrinsic in water resource management activities. Uncertainty arises from the incomplete information about the loads that a dam will actually experience, the lack of perfect information about the manner in which the dam will respond to those loads, and limited information about what the resulting consequences would be. The aim of seismic risk assessment is to identify loading conditions, potential failure modes, and consequences, and how to estimate the probabilities for each event. The overall process consists of hazard definition, seismic fragility, inventory data, and integration of the three. Among these components, the seismic fragility which associates structural failure with the level of ground motion is addressed in this paper. The seismic fragility of a dam is defined as the conditional probability of its failure at a given earthquake ground acceleration or spectral acceleration. The seismic fragility for gravity dams may be developed for various failure modes or limit states such as cracking, sliding, or rotational stability.

The objective of this study is to develop an efficient procedure in combination with the nonlinear structural analysis to develop seismic fragility for gravity dams. The seismic fragility for non-overflow gravity sections is developed in this paper and for the overflow sections including radial gates and piers in a future paper.

## 2. SEISMIC FRAGILITY METHODOLOGY

Seismic fragility analysis of structures is a time-variant reliability problem for which a closed form solution does not exist and, therefore simulation is inevitable. Full Monte Carlo Simulation (MCS) can produce most accurate results, but it requires an enormous amount of computational cost when

nonlinear time history analyses are involved. For most fragility analyses the pure random sampling of MCS may not be necessary, as long as distributions of the input parameters are reproduced accurately. Latin Hypercube Simulation (McKay et al., 1979), or LHS, is one such option that addresses this issue by providing a sampling method that appears random but also reproduces the input distributions with much greater efficiency than MCS.

The seismic fragility of the dam is developed based on definitions of failures that correspond to loss of water retention capability. Such failures could occur during the earthquake event if cracking due to ground shaking is significant and resistance to sliding and overturning is inadequate. They could also occur in the post-earthquake condition due to increased pore pressures in the cracks, loss of cohesion, and degradation of the friction coefficient as a result of seismic-induced displacements.

The seismic fragility of the dam is assessed by LHS method using nonlinear analyses that account for cracking, sliding, or rocking that could lead to a credible failure mode (Ghanaat et al., 2010). Fragility evaluations based on explicit nonlinear analysis are not common. A nonlinear response analysis is influenced by not only the various input parameters, but also by the characteristics of the specific earthquake record used as the seismic input. Thus nonlinear analyses must be repeated for each of the variables significant to seismic capacity and for multiple earthquake record time histories.

Implementation of the Separation-of-Variables Method (EPRI, 1994) in combination with nonlinear analysis would first require development and analysis of a model with median-centered properties. Because characteristics and phasing of the earthquake ground motion components can be significant to structure nonlinear response, analysis for multiple input time histories is necessary. To determine the variability in seismic capacity due to one of the significant variables, analysis using a model with the variable set to its 16% or 84% confidence value, with median values assigned to the other variables, would then be necessary. Such analyses must be repeated for each of the variables significant to seismic capacity and for multiple ground motion input levels to determine the failure capacity. It is apparent that a large number of nonlinear analyses could be necessary to implement the Separation-of-Variables Method. As a more efficient alternative when nonlinear analysis is required, seismic fragility evaluation of the dam is performed by LHS.

In the LHS Method, the number of trials, $N$, is first selected. $N$ sets of earthquake time histories are developed. Each set of time histories consists of two horizontal components and one vertical component. The median spectral accelerations of the $N$ sets of time histories should match the target ground motion response spectra over the frequency range significant to the response of the structure. $N$ probability bins are defined, with each bin having an equal probability of occurrence. For each variable significant to seismic capacity of the structure, values are assigned to each of the $N$ bins based upon the variable's probability distribution function. For the first trial, a value for each of the significant variables is randomly selected from the $N$ equal probability bins. One set of earthquake time histories is also randomly selected from the $N$ sets available. For the second trial, a value for each of the significant variables is randomly selected from the remaining $(N - 1)$ equal probability bins and one set of earthquake time histories is randomly selected from the remaining $(N - 1)$ sets. This process is repeated until the $N$ trials are populated.

In this study, a total of 10 trials was selected as being the minimum number capable of providing reasonably reliable results. For each of the 10 trials, values of significant parameters are randomly selected from their probability distributions. Structural models for each of the 10 trials are developed by inputting the values of the significant variables into the model. The seismic input acceleration time histories are scaled with random directionality factors before they are used in the seismic analysis. With the input parameters and seismic input established as discussed above, nonlinear seismic analysis trial runs for estimation of the seismic fragility are performed by increasing the intensity of the seismic input in each run until sliding failure of the dam is imminent. Nonlinear time-history analyses are then carried out with nonlinearity limited to the cracking and sliding along the dam base and at an upper lift-joint while the rest of the structure remains elastic. The peak ground acceleration

corresponding to the failure point represents the seismic capacity of the structure for that particular trial.

## 3. SEISMIC EVALUATION INPUT PARAMETERS

Based on the experience in seismic response behavior of concrete dams, the following 11 randomness and uncertainty variables are considered to be most significant to dam seismic capacity: 1) earthquake ground motion time histories, 2) concrete elastic modulus, 3) rock elastic modulus, 4) concrete damping, 5) lift-joint tensile strength, 6) lift-joint friction angle, 7) lift-joint cohesion, 8) concrete-rock interface tensile strength, 9) concrete-rock interface friction angle, 10) concrete-rock interface cohesion, and 11) drain efficiency.

### 3.1 Earthquake ground motion – randomness variable

The variability of earthquake ground motion was accounted for by using 10 different sets of ground motion records from earthquake events whose magnitudes and source-to-site distances were consistent with the dam site, but represented different ground motion characteristics in terms of duration, pulse characteristics, pulse sequencing, etc. The earthquake time history records were obtained from the Pacific Earthquake Engineering Research (PEER, 2005) Ground Motion Database. The acceleration time histories were selected from earthquake magnitudes in the range of M6.0 to M6.75, source-to-site distances up to 20.5 km, and strike-slip plus reverse/oblique fault types consistent with design ground motions of the dam. The time histories were modified to match the design response spectrum, but for fragility analysis they were further modified by directionality factors to account for variability of horizontal and vertical components of the earthquake ground motion in a systematic manner.

Because the LS-DYNA model (see Section 4.2) includes non-reflecting boundaries, seismic input must consist of stress time histories rather than acceleration time histories. This was accomplished in several steps: 1) the ground-surface acceleration time histories were de-convolved to obtain acceleration time histories at the bottom of the model, 2) velocity time histories at the bottom of the model were obtained by integrating the acceleration time histories from Step 1, and 3) the velocity time histories were then converted to stress time histories using $\sigma_s = 2(\rho c_s)v_s$ for shear stress and $\sigma_n = 2(\rho c_n)v_s$ for normal stress. Where $\rho$ = mass density of the foundation rock, $c_s$ = shear wave velocity of the foundation rock, $c_n$ = compression wave velocity in foundation, $v_s$ = horizontal ground velocity at the bottom, and $v_n$ = vertical ground velocity at the bottom.

### 3.2 Uncertainty variables

These variables are the only input parameters whose uncertainty or likelihood of occurrence is formally included in the analysis. All other input parameters are kept constant and represented by their best estimate values. The likelihood of a variable having a certain value is determined from probability distribution function (PDF) assigned to that variable. The PDF for a variable may be defined by statistical methods if sufficient data are available, or assumed based on experience or knowledge of low, best-estimate, and high values of the variable.

The median and coefficient of variation of certain variables were available from the test of concrete and rock cores. Thus they data were used to develop a lognormal PDF for the concrete modulus, rock modulus, and tensile strengths of the lift-joint and concrete-rock interface. The PDF for each variable was then divided into 10 equal probability intervals to generate values for that particular variable as input to the analysis. The damping ratio was also represented by a lognormal PDF to generate 10 values ranging from 2.8 to 8.9 percent.

The measured data were limited for shear strengths of the lift-joint and concrete-rock interface and did not exist for the drain efficiency. For these variables, a triangular PDF defined by the minimum, most likely, and maximum estimates was used to generate 10 equal-probability values needed for the

analysis. The minimum, most likely, and maximum estimates for cohesion and friction angle were obtained from available test results and for drain efficiency they were assumed equal to 0, 50%, and 75%, respectively.

## 4. FINITE-ELEMENT MODEL

### 4.1 Dam description

The gravity dam section used in this study is similar to the tallest non-overflow section at an Example Dam. The Example Dam consists of 28 individual monoliths, each 50 feet in width (Figure 4.1). The selected monolith rises 336.50 feet above the base from El. 144 to El. 480.50 feet. It is 32 feet wide at the crest and 251.80 feet at the base. It is sloped at 0.7H:1.0V on the downstream and 0.1H:1.0V on the upstream side. The upstream-face incline changes to vertical at elevations above 408 feet, and the downstream slope converts to vertical gently through a circular curve.

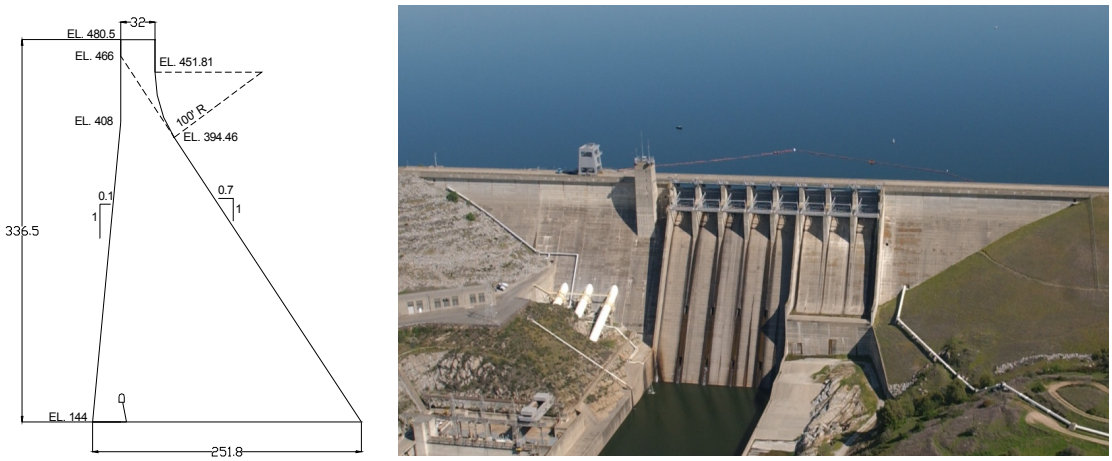


**Figure 4.1.** Example Dam and geometry of tallest non-overflow section.

### 4.2 Model configuration and boundary conditions

The seismic fragility of the selected non-overflow gravity section is evaluated for a single monolith with movements constrained to the upstream-downstream and vertical directions. The model is a 50-foot-thick 3D slice which includes a portion of the headwater and the foundation rock (Figure 4.2) and is developed using the computer program LS-DYNA (LSTC, 2008). The dam is modeled using 4,816 3D solid elements in 8 layers through the monolith thickness with concrete material properties. The effects of dam-water interaction are fully accounted for by modeling the headwater using 3,780 3D compressible fluid elements with water properties. Non-reflecting boundary conditions are introduced at the upstream extent of the fluid domain to allow for transmission of water pressure waves propagating away from the dam. The effects of dam-foundation interaction are also fully considered by a foundation model that includes the inertia, flexibility, and damping effects. This is accomplished by modeling the foundation as part of the dam model and introducing non-reflecting boundary conditions at the bottom and the upstream and downstream surfaces of the foundation model to simulate a semi-infinite response behavior without extending the mesh to large distances from the dam. The foundation model consists of 10,944 3D solid elements with rock properties arranged in 8 to 4 to 2 layers through the monolith width from top of the rock to bottom of the foundation model.

### 4.3 Model nonlinearity – potential failure modes

Tensile cracking at the base of the dam and at the upper lift joints are two common potential failure modes for a typical non-overflow gravity dam section. These cracks if extended through the dam section could lead to sliding and rotation at the cracked base and lift-joint. The credibility of these

potential failure modes was first verified by nonlinear analyses of all 10 trial models before proceeding with the fragility analysis. The verification nonlinear analyses were carried out using the Winfrith (Broadhouse, 1995) nonlinear concrete model, which permits tensile cracking of the dam mass concrete. All 10 nonlinear analyses, each having different material properties and ground motion time histories, indicated that tensile cracking always occurs at the dam-foundation interface and at an upper lift-joint near the change of slope.

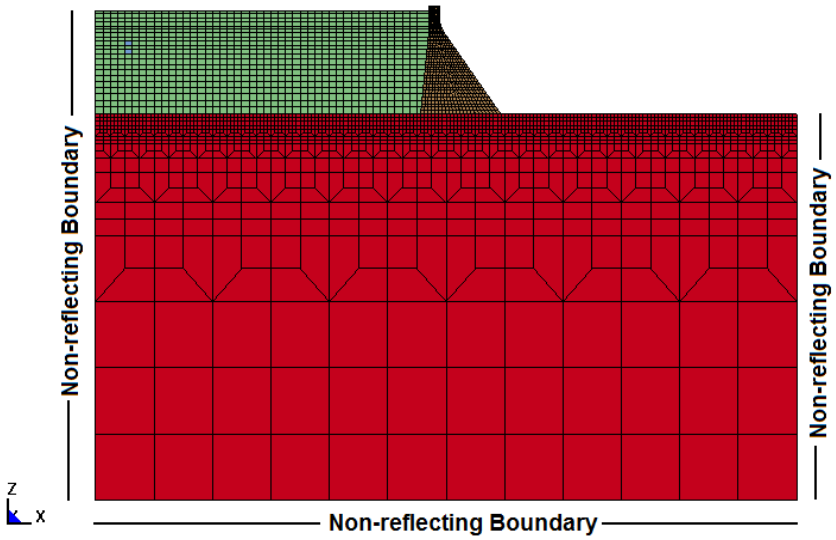


**Figure 4.2.** Dam-water-foundation model with non-reflecting boundaries.

### 4.4 Nonlinear model for seismic fragility

Based on findings of the verification analyses, all subsequent seismic fragility analyses were accomplished by limiting concrete cracking and failure to the dam-foundation interface and the upper lift-joint, while the rest of the dam section assumed to behave linearly. These potential failure mechanisms were modeled using the tiebreak contact elements available in LS-DYNA. A tiebreak contact element allows the modeling of interfaces that transmit compressive, tensile, and shear forces until failure, resulting in a tie. The break part of the contacts allows the modeling of shear break and tensile cracking, causing independent motions of the nodes on either side of the interface (Figure 4.3). The post-failure response of a tiebreak contact is the same as the traditional compression-only contacts where shear resistance is limited to frictional force and tensile resistance is zero. The potential slip surfaces modeled by the tiebreak contacts represent the regions exhibiting nonlinear response behavior (Figures 4.3). The tiebreak contacts initially tie the upper and lower slip surfaces together until the interface tensile and shear stresses satisfy the tension-shear criteria given on Figure 4.3. Where $\sigma_n$ is the interface normal stress, $\sigma_s$ is the interface shear stress, *NFLS* is the normal failure limit stress (i.e., tensile strength), and *SFLS* is the shear failure limit stress (i.e., cohesion). The dam-foundation interface was populated with 176 contact elements, 22 through the dam thickness by 8 across the monolith width. The lift-joint included 64 contact elements, 8 through the dam thickness by 8 across the monolith width. The use of numerous contact elements through the dam thickness facilitated the formation and gradual propagation of the shear break and tensile cracking.

## 5. NONLIENAR SEISMIC ANALYSIS

The seismic performance and the likelihood of dam failure are appraised by the available capacity to resist the seismic demand. Under static loads and in the absence of cracking the dam section maintains its full capacity to resist sliding and overturning. In this case, the shear resistance along the potential failure surfaces includes both the friction and cohesion. However, additional demands by the seismic

loads induce cracking and diminish cohesion in the cracked region. As the cracks propagate, the available capacity reduces more and more, due to loss of cohesion. Ultimately, only frictional resistance at the base and along lift joints will be available to withstand the shear demands. The failure or limit state occurs as soon as the shear capacity drops below the shear demand and the dam or the upper isolated block begins sliding and/or rocking.

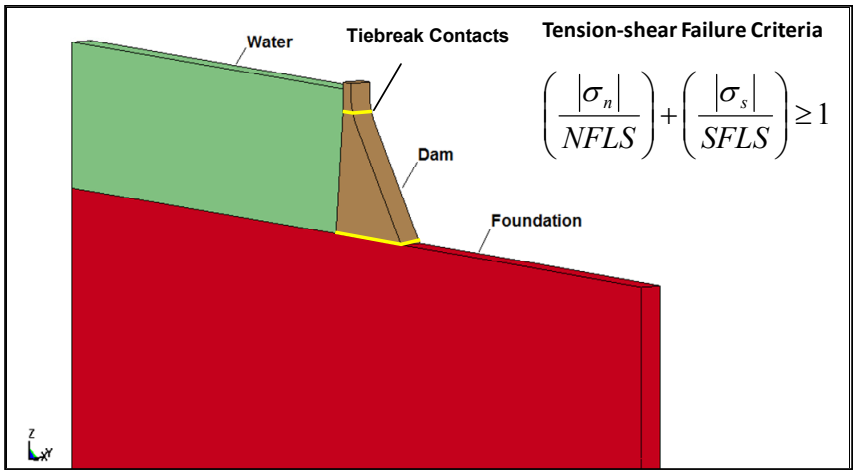


**Figure 4.3.** Nonlinear model with tiebreak contacts at upper lift-joint and base of dam.

In all 10 trial runs, the limit state or failure involved tensile cracking that started from the upstream or downstream face of the dam and propagated along the base or the lift joint, followed by sliding and rocking. In four of the trials the sliding initiated first at the base and then at the lift joint after the ground motion intensity was increased. In the remaining six trials, the sliding initially occurred at the lift-joint and later at the base when the ground motion intensity was increased. The sliding at the lift-joint was accompanied with significant rocking of the upper block that exacerbated the sliding. The sliding at the base also generated some modest rocking of the dam section but much less than the upper block.

Table 5.1 summarizes peak values of accelerations and sliding displacements at failure point. The accelerations in Column 3 represent the peak ground accelerations at which the sliding was first observed at the base and/or the lift-joint. These were obtained running successive nonlinear analyses for each trial by scaling the input time histories to peak ground accelerations in the range of 0.05g to 1.10g until sliding occurred at the base and/or the lift-joint. For each trial, the lower peak acceleration value indicates the acceleration at which the sliding was first observed either at the base or at the lift-joint. The higher peak acceleration value represents the acceleration at which the sliding was first observed at both the base and upper block. The failure mode and the sequence of sliding are briefly described in Column 4. The table also summarizes the amount of sliding displacements or permanent movements corresponding to the first occurrence of sliding at one or both locations. They vary from 1.15 inches to 23.28 inches at the base and 0.1 inches to 31.8 inches at the upper block.

Figures 5.1 and 5.2 illustrate the results for Trial-6 at 1.10g ground motion level. Figure 5.1 exhibits a snap shot of the horizontal displacement contours. A shift or distinct colors on either side of the dam-foundation interface or the lift joint indicate relative movements or sliding at that location. For example, sliding at the lift-joint is evident by the blue and red colors and visible dislocation of the upper block, and at the base by different shades of blue. Figure 5.2 provides a sample of time histories for the base and lift-joint sliding displacements. The results also indicate that the upper block and dam section interact dynamically during the earthquake ground shaking. The base sliding, when occurs first, could delay and possibly eliminate sliding of the upper block. This interaction is believed to be affected by the intensity and characteristics of the ground motion. A clear example of this interaction

can be observed for Trial 4 in Table 5.1. At 0.48g, both the dam section and upper block slide, showing 0.75 and 0.10 inches of permanent displacement, respectively. At 0.50g, the upper block undergoes rocking but not sliding, while the dam section indicates 10.45 inches of sliding. Increasing the ground motion intensity to 0.6g (results not shown) induced sliding both at the base and at the upper block.

**Table 5.1.** Summary results of trial runs at failure (sliding at base or lift joint or both).

| Trial No. | TH No. | Failure Peak Acc. | Failure Mode | Sliding Disp. (in) | |
|---|---|---|---|---|---|
| | | | | Base | Lift Joint |
| 1 | TH01 | 0.10g | Sliding at base only | 1.00 | 0.00 |
| | | 0.13g | Sliding first at base then at lift joint | 1.15 | 1.18 |
| 2 | TH02 | 0.28g | Sliding at lift joint only | 0.00 | 3.15 |
| | | 0.29g | Sliding first at lift joint then at base | 10.37 | 3.05 |
| 3 | TH03 | 0.70g | Sliding at lift joint only | 0.00 | 2.37 |
| | | 0.80g | Sliding first at lift joint then at base | 15.84 | 31.8 |
| 4 | TH04 | 0.48g | Sliding first at base then at lift joint | 1.75 | 0.10 |
| | | 0.50g | Sliding at base and rocking at lift joint | 10.45 | 0.00 |
| 5 | TH05 | 0.42g | Sliding at lift joint only | 0.00 | 3.54 |
| | | 0.50g | Sliding first at lift joint then at base | 0.97 | 5.42 |
| 6 | TH06 | 1.05g | Sliding at lift joint only | 0.00 | 9.93 |
| | | 1.10g | Sliding first at lift joint then at base | 3.20 | 11.53 |
| 7 | TH07 | 0.10g | Sliding at base only | 3.70 | 0.00 |
| | | 0.50g | Sliding first at base then at lift joint | 18.00 | 1.56 |
| 8 | TH08 | 0.19g | Sliding at base only | 1.18 | 0.00 |
| | | 0.26g | Sliding first at base then at lift joint | 2.40 | 2.10 |
| 9 | TH09 | 0.60g | Sliding at lift joint only | 0.00 | 4.9 |
| | | 0.65g | Sliding first at lift joint then at base | 3.33 | 5.71 |
| 10 | TH10 | 0.55g | Sliding at lift joint only | 0.00 | 4.72 |
| | | 0.60g | Sliding first at lift joint then at base | 23.28 | 6.58 |

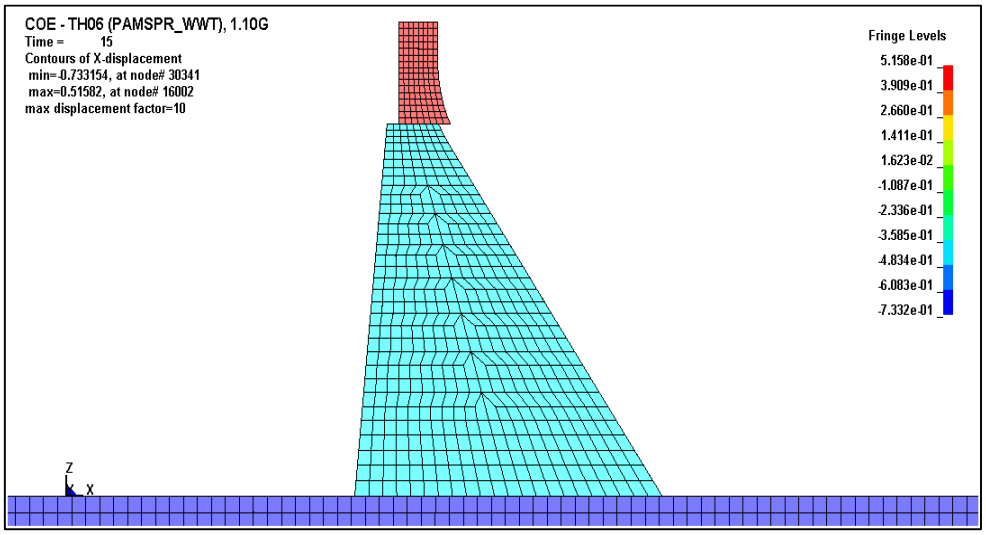


**Figure 5.1.** Trial-6 – Dam slides at base and lift-joint with time history scaled to 1.10g.

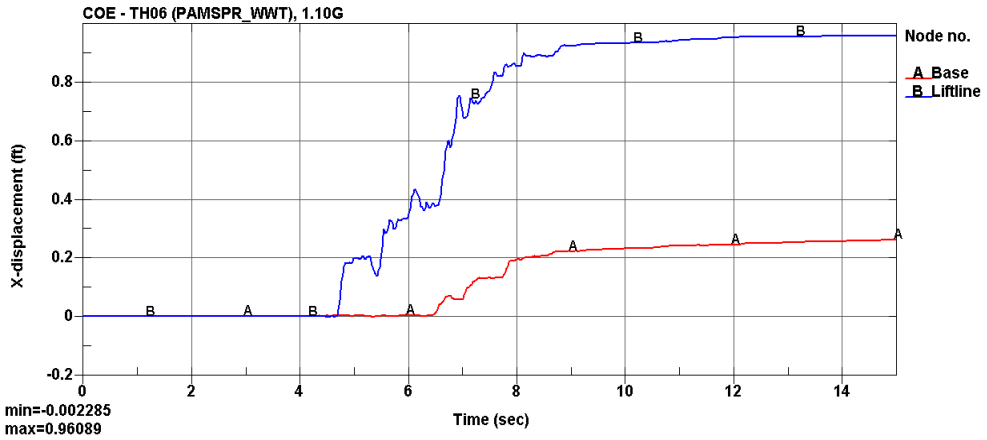


**Figure 5.2.** Trial-6 – Time histories of base and lift-joint sliding displacements at 1.10g.

## 6. SEISMIC FRAGILITY DEVELOPMENT

For the 10 Latin-Hypercube random nonlinear trials, the peak acceleration capacity associated with the incipient sliding of the dam section or the upper block are listed in Table 6.1 from low to high values. The non-exceedance probability (NEP) for each trial, also listed in the table, is given by:

$$NEP = 100\% \left( \frac{n - 0.5}{N} \right) \tag{7.1}$$

Where $N$=10 trials, and $n$ is the ordered trial number. The failure (or limit state) probability $P_F$ as a function of peak acceleration capacity is:

$$P_F = NEP \tag{7.2}$$

**Table 6.1**. Failure probability ($P_F$) as function of failure peak acceleration capacity ($A_c$).

| n | Base Sliding Failure Peak Acc. (g) | Lift-joint Sliding Failure Peak Acc. (g) | $P_F$ = NEP (%) |
|---|---|---|---|
| 1 | 0.015 | 0.12 | 5 |
| 2 | 0.019 | 0.235 | 15 |
| 3 | 0.19 | 0.24 | 25 |
| 4 | 0.29 | 0.25 | 35 |
| 5 | 0.45 | 0.26 | 45 |
| 6 | 0.49 | 0.35 | 55 |
| 7 | 0.60 | 0.40 | 65 |
| 8 | 0.65 | 0.45 | 75 |
| 9 | 0.73 | 0.50 | 85 |
| 10 | 1.05 | 0.60 | 95 |

Figure 6.1 provides a cumulative normal plot of failure probability ($P_F$) for base sliding versus failure peak acceleration ($A_c$). The data fits quite well with the following Weibull distribution:

$$P_F = 1 - \exp\left[-\left(\frac{A_c}{\beta}\right)^{\alpha}\right] = 1 - \exp\left[-\left(\frac{A_c}{0.54}\right)^{1.44}\right] \tag{7.3}$$

In Eqn. 7.3, $\alpha$ is the shape parameter (or slope) and $\beta$ is the scale parameter of the distribution. The median seismic fragility and standard deviation for the base sliding are determined to be 0.42g and 0.35, respectively. The *R*-squared or coefficient of determination between the data and the Weibull distribution is 0.9517, signifying a very good fit.

Figure 6.2 provides a similar cumulative normal plot of failure probability ($P_F$) for the lift-joint sliding as a function of failure peak acceleration ($A_c$). The data for lift-joint sliding also fits very well with the following Weibull distribution:

$$P_F = 1 - \exp\left[-\left(\frac{A_c}{\beta}\right)^{\alpha}\right] = 1 - \exp\left[-\left(\frac{A_c}{0.38}\right)^{2.4}\right] \tag{7.4}$$

From the distribution the median seismic fragility and standard deviation for the lift-joint sliding are calculated to be 0.33g and 0.15, respectively. The *R*-squared or coefficient of determination between the data and the Weibull distribution is 0.96, indicating an excellent fit.

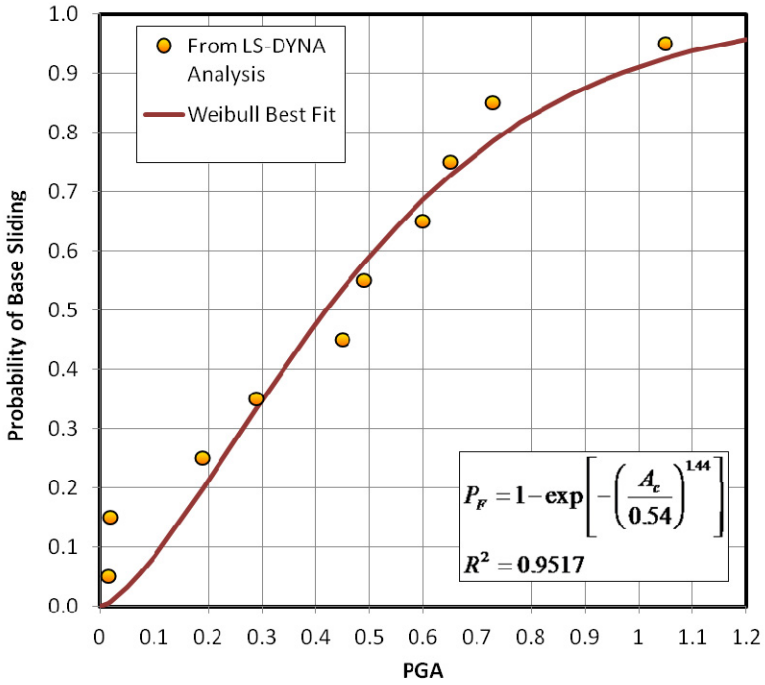


**Figure 6.1.** Plot of failure (base sliding) probability versus failure peak acceleration.

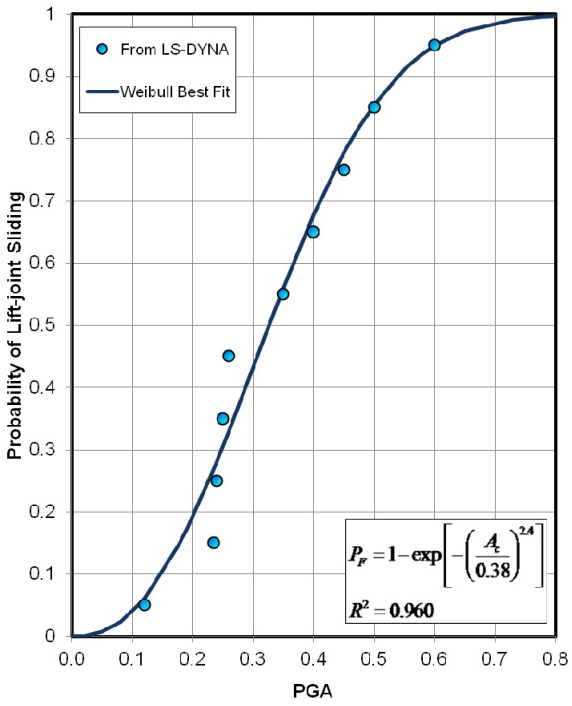


**Figure 6.2.** Plot of failure (Lift-joint sliding) probability versus failure peak acceleration.

## 7. CONCLUSION

This paper presented a practical methodology for development of seismic fragilities for concrete gravity dams using nonlinear time-history analysis with Latin Hypercube Simulation. The methodology uses advanced nonlinear analysis with structural failure capability and considers full dam-water and dam-foundation interaction effects. The seismic fragilities obtained for the base and lift-joint sliding of the example dam are reasonable and fit quite well with the Weibull probability distribution. The results indicate a median seismic fragility of 0.42g for sliding at the base of the dam with a standard deviation of 0.35. The seismic fragility for sliding at the uplift-joint was found to be 0.33g with a standard deviation of 0.15.


### ACKNOWLEDGEMENTS

The writers acknowledge the financial support of the US Army Corps of Engineers, Headquarters, Washington D.C. The view of the authors does not purport to reflect the positions of the Department of the Army or the Department of Defense.


### REFERENCES


Broadhouse, B.J. (1995). The Winfrith Concrete Model in LS-DYNA3D. *Report:* ***SPD/D(95)363***, Structural Performance Department, AEA Technology, Winfrith Technology Centre, U.K.

EPRI (1994). Methodology for developing seismic fragilities. EPRI Report **TR-103959**, Palo Alto, CA.

Ghanaat, Y., Hashimoto, P.S., Zuchuat, O., and Kennedy, R.P. (2011). Seismic fragility of Mühleberg Dam using nonlinear analysis with Latin Hypercube Simulation. *Proceedings of the* ***31st*** *Annual USSD Conference*, San Diego, California, April 11-15, 2011.

LSTC (2008). *LS-DYNA*, Version ls971s R2, Livermore Software Technology Corp. Livermore, CA.

McKay, M.D., Beckman, R.J., and Conover, W.J. (1979). A Comparison of three methods for selecting values of input variables in the analysis of output from a computer code. *Technometrics*, **21**, 239-245.

PEER (2005). Pacific Earthquake Engineering Center. *PEER NGA Data Set*, **Version 5.0,** University of California, Berkeley.